

# Trace anomaly contributions to baryon masses from Lattice QCD (CLQCD Collaboration)



Bolun Hu,<sup>1</sup> Xiangyu Jiang,<sup>1</sup> Keh-Fei Liu,<sup>2,3</sup> Peng Sun,<sup>4</sup> and Yi-Bo Yang<sup>1,5,6,7,\*</sup>

<sup>1</sup>*CAS Key Laboratory of Theoretical Physics, Institute of Theoretical Physics,  
Chinese Academy of Sciences, Beijing 100190, China*

<sup>2</sup>*University of Kentucky, Lexington, KY 40506, USA*

<sup>3</sup>*Nuclear Science Division, Lawrence Berkeley National Laboratory, Berkeley, California 94720, USA*

<sup>4</sup>*Institute of Modern Physics, Chinese Academy of Sciences, Lanzhou, 730000, China*

<sup>5</sup>*University of Chinese Academy of Sciences, School of Physical Sciences, Beijing 100049, China*

<sup>6</sup>*School of Fundamental Physics and Mathematical Sciences,*

*Hangzhou Institute for Advanced Study, UCAS, Hangzhou 310024, China*

<sup>7</sup>*International Centre for Theoretical Physics Asia-Pacific, Beijing/Hangzhou, China*

(Dated: November 28, 2024)

We present lattice calculations of the masses of baryons containing the light, strange and charm quarks and their decompositions into sigma terms and trace anomaly. These results are obtained from 2+1 flavor QCD ensembles at 5 lattice spacings  $a \in [0.05, 0.11]$  fm, 4 spatial sizes  $L \in [2.5, 5.1]$  fm, 7 pion masses  $m_\pi \in [135, 350]$  MeV, and several values of the strange quark mass. The continuum extrapolated masses of all the baryons agree with experiments at the 1% level. We found that the glue part of the trace anomaly contributes about the same amount to the masses –  $\sim 0.8 - 0.95$  GeV for the spin 1/2 baryons and  $\sim 0.95 - 1.1$  GeV for the spin 3/2 baryons – given  $\gamma_m \sim 0.3$ , and the sigma terms from the light, strange, and charm quarks are enhanced by factors of about 5, 2, and 1.3, respectively, compared to the renormalized quark mass themselves at  $\overline{\text{MS}}$  2 GeV.

*Introduction:* Based on the standard model of particle physics, the interactions between fundamental particles and the Higgs boson are responsible for the origin of their masses. However, the Higgs mechanism is known to affect certain particles much more than others; for example, the mass of the heaviest flavor of quark can be  $10^5$  times greater than that of the lightest flavor [1]. This disparity presents a central puzzle within the standard model.

This puzzle becomes even more complex when the gluons combine the quarks into hadrons through the strong interaction. Current collinear experiments have confirmed over 500 hadrons with various masses, which, in principle, should be determined by no more than seven parameters: the masses of all quarks except the top quark (which decays rapidly), the strong coupling constant  $\alpha_s$ , and the electromagnetic coupling constant  $\alpha \sim 1/137$ . While  $\alpha$  can only influence hadron masses at a 1% level, it can be crucial in certain cases like the mass splitting between neutrons and protons [2].

In the framework of quantum field theory, hadron mass is associated with the breaking of scale invariance in the energy-momentum tensor (EMT)  $T^{\mu\nu}$ . At the classical level, this corresponds solely to the quark mass contri-

butions. However, at the quantum level, it also includes additional trace anomalies arising from the scale non-invariance of the quark masses  $m_f$  and the strong coupling constant  $\alpha_s$  [3–5]:

$$m_H = T_\mu^\mu = \sum_f m_f \langle \bar{q}_f q_f \rangle_H + \left\langle \frac{\beta(\alpha_s)}{2\alpha_s} F^{\mu\nu} F_{\mu\nu} + \sum_f \gamma_m m_f \bar{q}_f q_f \right\rangle_H, \quad (1)$$

where  $\langle O \rangle_H \equiv \langle H|O|H \rangle / \langle H|H \rangle$ ,  $m_H$  is the hadron mass,  $\gamma_m = \frac{2}{\alpha_s} \alpha_s + \mathcal{O}(\alpha_s^2)$  is the quark mass anomalous dimension,  $F^{\mu\nu}$  is the gluon field strength tensor, and  $\beta$  is the anomalous dimension of  $\alpha_s$ . Therefore, the Higgs contribution to hadron mass via quark mass is enhanced by a factor of  $(1 + \gamma_m) \langle \bar{q}q \rangle_H$ , reflecting the additional contributions from quark-antiquark pairs, while the remaining part originates purely from the strong interaction through the condensation of massless gluons within the hadron. Three-quarters of the trace anomaly contribution can be further decomposed into the quark and gluon kinetic energies through the sum rule of the QCD Hamiltonian [6, 7].

Previous lattice QCD calculations and phenomenological analyses of experimental data have confirmed that the contributions of up and down quarks to the lightest

\* Corresponding author: [ybyang@itp.ac.cn](mailto:ybyang@itp.ac.cn)

baryon, the nucleon, range from 40 to 70 MeV [8–19]. This enhancement results in the Higgs contribution being increased by a factor of approximately 4 to 7, based on the light quark mass at  $\overline{\text{MS}}$  2 GeV [20]. The contribution from the strange quark is also significant, approximately 40 MeV [8–12, 21, 22], which corresponds to about 40% of  $m_s^{\overline{\text{MS}}}$  (2 GeV). Recent direct calculations of the gluon trace anomaly contribution [23] have verified that the gluon trace anomaly accounts for most of the nucleon mass, while its contribution is much smaller for the pseudo-Goldstone boson of QCD, namely the pion, which approaches zero as the quark mass becomes negligible. Further studies of the spatial distribution [23] and form factors [24] suggest the existence of a negative mass hollow in the center of the pion due to the trace anomaly, distinguishing its mass from that of other hadrons. Based on the sum rule of the EMT form factors [25], these observations have been indirectly confirmed through form factor calculations of the off-diagonal part of the EMT [26, 27], and then can be accessible from the future collinear experiments.

But how the Higgs and gluon coupling to the quarks affect the other hadron masses are still far from clear. The quark model suggests that the enhancement of strong interaction on the quark mass contribution to the hadron mass should be significantly weakened for the heavier quark flavors, while the quantitative estimate of the trace anomaly contribution to the baryon with heavy quark flavor is absent. In this work, we present the first quantitative prediction of the quark mass and gluon trace anomaly contributions to the  $J = 1/2$  and  $3/2$  ground state baryons from the first principle lattice QCD calculation, with the systematic uncertainty from nonphysical quark mass, continuum and infinite volume extrapolations under control.

*Numerical setup:* The ensembles used in this work are summarized in Table I. They were generated using a 2+1 flavor clover fermion action and with a tadpole-improved Symanzik gauge action. Based on the joint fit on subsets of these ensembles with several lattice spacing, quark masses and volumes [28, 29], the physical up, down, strange and charm quark masses and also related CKM matrix elements  $V_{u(c)d(s)}$  agree with the current lattice averages well [30]. These ensembles have been also used to study the hadron spectrum [31–35] and structures [36–39].

For the interpolation fields of the baryons, we use  $\epsilon_{abc}P^+ [(q_a^1)^T C \gamma^5 q_b^2] q_c^3$  and  $\epsilon_{abc}P^+ [(q_a^1)^T C \gamma^\mu q_b^2] q_c^3$  for the spin-1/2 and 3/2 particles, respectively. Note that some of the particles require linear combination of different permutations of three quarks, which are detailed in the supplemental materials [40]. As presented in Table I, we computed the Coulomb gauge fixed source propagators at  $n_{\text{src}}^l$  time slices for each configuration at three light quark masses including the unitary one, and at  $n_{\text{src}}^{s,c}$  for three strange and charm quark masses. We have 23,845 (for the proton and  $\Delta$  baryon) and 17,725 (for the other baryons) measurements on the 3,340 configurations of 14

ensembles in total. The other information of the ensembles we used in this work are outlined in Table I, and we use  $\tilde{O}$  for the dimensionless value of any quantity  $O$ .

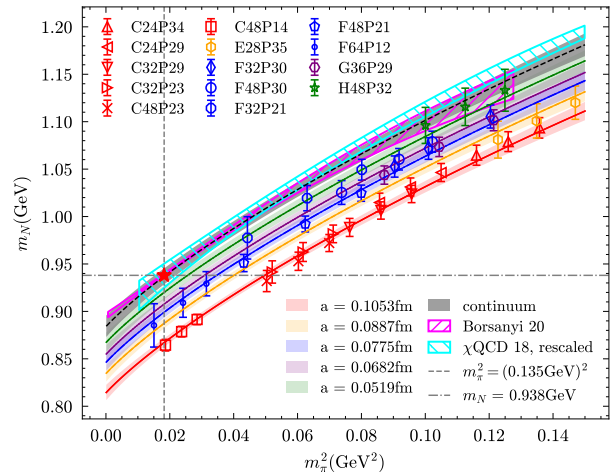


FIG. 1. The nucleon mass on 14 ensembles at 5 lattice spacings (colored data points and bands), and also that in the continuum (gray band). The mismatch effect from the unequal valence and sea pion masses has been corrected based on the joint fit. The continuum extrapolated results using the overlap fermion [7] (rescaled to match the physical nucleon mass) and staggered fermion [41] are also illustrated for comparison.

The masses of the ground state baryons are extracted from fits of the two-point correlation functions. We fit the nucleon mass using the the SU(4|2) partially quenched heavy baryon chiral perturbative theory ( $\chi$ PT) ansatz [7, 42],

$$\begin{aligned}
 m_H(m_\pi^{\text{val}}, m_\pi^{\text{sea}}, m_{\eta_s}^{\text{sea}}, a, L) &= m_H^{\text{phys}} \\
 &+ \sum_{\text{tag=val/pq}, j=2,3} C_j^{\text{tag}} [(m_\pi^{\text{tag}})^j - (m_\pi^{\text{phys}})^j] \\
 &+ C_s [(m_{\eta_s}^{\text{sea}})^2 - (m_{\eta_s}^{\text{phys}})^2] \\
 &+ C_L \frac{(m_\pi^{\text{val}})^2}{L} e^{-m_\pi^{\text{val}} L} + \sum_i C_a^{2i} a^{2i}, \quad (2)
 \end{aligned}$$

where  $m_\pi^{\text{val}}$  and  $m_\pi^{\text{sea}}$  are the valence and sea pion masses respectively,  $m^{\text{pq}} = \sqrt{(m_\pi^{\text{val}})^2 + (m_\pi^{\text{sea}})^2}$  is the partially quenched pion mass,  $m_\pi^{\text{phys}} = 134.98$  MeV is the physical  $\pi^0$  mass, and  $m_{\eta_s}^{\text{phys}} = 689.89(49)$  MeV from Ref. [43] is the pure QCD  $\eta_s$  mass which corresponds to the physical strange quark mass.

In Fig. 1, we present the nucleon mass at five different lattice spacings as colored data points, with the mismatch effects between  $m_\pi^{\text{val}}$  and  $m_\pi^{\text{sea}}$  are corrected using the joint fit which gives  $\chi^2/\text{d.o.f.} = 1.2$ . Redefinition of parameters  $C_3^{\text{val}} = \frac{(g_A^2 - 4g_A g_1 - 5g_1^2)\pi}{3(4\pi f_\pi)^2}$  and  $C_3^{\text{pq}} = \frac{(8g_A^2 + 4g_A g_1 + 5g_1^2)\pi}{3(4\pi f_\pi)^2}$  are used to be consistent with the previous studies [7, 42]. The colored bands corresponds to

TABLE I. Lattice size  $\tilde{L}^3 \times \tilde{T}$ , gauge coupling  $\hat{\beta}$ , bare quark mass parameters  $\tilde{m}_{l,s}^b$ , the corresponding pseudoscalar mass  $m_{\pi,\eta_s}$ , and the statistics information.

Symbol	$\tilde{L}^3 \times \tilde{T}$	$\hat{\beta}$	$a$ (fm)	$\tilde{m}_l^b$	$\tilde{m}_s^b$	$m_\pi$ (MeV)	$m_{\eta_s}$ (MeV)	$m_\pi L$	$n_{\text{cfg}}$	$n_{\text{src}}^l$	$n_{\text{src}}^{s,c}$
C24P34	$24^3 \times 64$	6.20	0.10521(11)(62)	-0.2770	-0.2310	340.2(1.7)	748.61(75)	4.38	199	32	32
C24P29	$24^3 \times 72$			-0.2770	-0.2400	292.3(1.0)	657.83(64)	3.75	760	3	3
C32P29	$32^3 \times 64$			-0.2770	-0.2400	293.1(0.8)	658.80(43)	5.01	489	3	3
C32P23	$32^3 \times 64$			-0.2790	-0.2400	227.9(1.2)	643.93(45)	3.91	400	3	3
C48P23	$48^3 \times 96$			-0.2790	-0.2400	224.1(1.2)	644.08(62)	5.79	60	3	3
C48P14	$48^3 \times 96$			-0.2825	-0.2310	136.4(1.7)	706.55(39)	3.56	136	48	3
E28P35	$28^3 \times 64$	6.308	0.08970(26)(53)	-0.2490	-0.2170	351.4(1.4)	717.94(93)	4.43	142	4	4
F32P30	$32^3 \times 96$	6.41	0.07751(14)(45)	-0.2295	-0.2050	300.4(1.2)	675.98(97)	3.81	250	3	3
F48P30	$48^3 \times 96$			-0.2295	-0.2050	302.7(0.9)	674.76(58)	5.72	99	3	3
F32P21	$32^3 \times 64$			-0.2320	-0.2050	210.3(2.3)	658.79(94)	2.67	194	3	3
F48P21	$48^3 \times 96$			-0.2320	-0.2050	207.5(1.1)	661.94(64)	3.91	75	3	3
F64P12	$64^3 \times 128$			-0.2336	-0.2030	122.8(0.9)	679.90(30)	3.09	109	4	4
G36P29	$36^3 \times 108$	6.498	0.06884(18)(41)	-0.2150	-0.1926	297.2(0.9)	693.05(46)	3.68	270	4	4
H48P32	$48^3 \times 144$	6.72	0.05198(20)(31)	-0.1850	-0.1700	316.6(1.0)	691.88(65)	4.06	157	12	12

the fit prediction at respective lattice spacings, and they agree with the data points well. Based on the linear  $a^2$  extrapolation, our continuum extrapolated result as function of pion mass is shown as gray band, which perfectly agree with the that from using the overlap fermion [7] and staggered fermion [41]. The physical nucleon mass is shown as the red star. Note that the band from Ref. [7] is rescaled by  $1.5\sigma$  from the original data to match the physical point.

For the light baryons containing a strange quark, we calculate the baryon masses using three different strange quark masses for each ensemble. We then interpolate the strange quark mass to the value corresponding to the artificial  $\eta_s$  (unmixed  $\bar{s}s$ ) mass  $m_{\eta_s}^{\text{phys}} = 689.89(49)$  MeV [43], which is determined by using the physical strange quark mass and is consistent with the value of  $687.4(2.2)$  MeV [28] obtained from CLQCD ensembles, albeit with a larger uncertainty.

The cases of charmed baryons are also similar. Following the the GRS renormalization scheme  $m_{q,\text{QCD+QED}}^{\overline{\text{MS}}}(2\text{GeV}) = m_{q,\text{QCD}}^{\overline{\text{MS}}}(2\text{GeV})$ , we use the pure QCD value  $m_{D_s} = 1966.7(1.5)$  MeV [44] to determine the interpolated valence charm quark mass for each ensemble. The resulting masses of open and closed charmed mesons, as well as their decay constants, agree well with experimental values and lattice averages [29].

The interpolation of valence strange and charm quark masses significantly suppresses the discretization errors from the heavy quark and also allows us to use a similar ansatz as that used for nucleons to fit the baryon mass for different flavors and angular momentum. For the charmed baryon, we retain the  $a^4$  term in the extrapolation, as the linear  $a^2$  extrapolation does not describe the data well, resulting in poor  $\chi^2$ . We also take  $m_\pi^{\text{val}} = m_\pi^{\text{sea}}$  and drop the  $(m_\pi^{\text{tag}})^{2,3}$  terms for baryon without valence light quark.

In Fig. 2, we show the lattice spacing dependence of the nucleon,  $\Omega$  and  $\Omega_c$  masses, with the light and strange

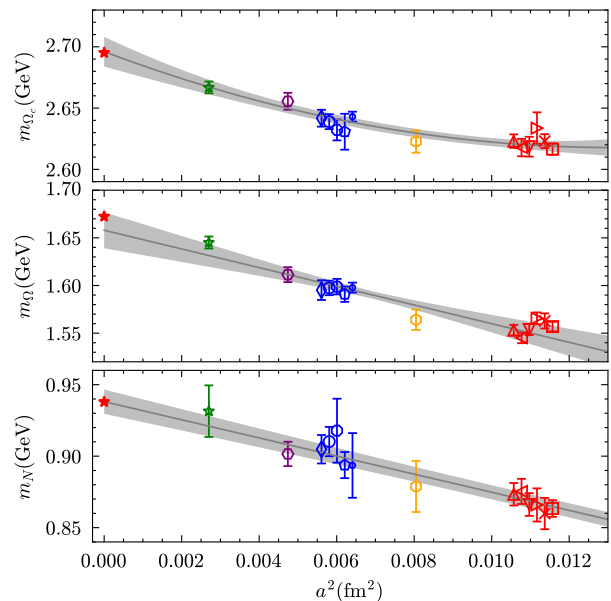


FIG. 2. Fitting results for nucleon,  $\Omega$ , and  $\Omega_c$  masses as functions of  $a^2$ . The other non-physical effects for the data points are fixed using the global fit.

quark masses corrected to their physical value based on the joint fit on 14 ensembles. The gray bands indicate the fit uncertainties, and the red stars correspond to the experimental values. Obviously the linear  $a^2$  dependence describe the data of nucleon and  $\Omega$  well, while the  $a^4$  term is essential for the  $\Omega_c$ . For a comprehensive view, the results for the other baryons and also more information on our ground state extraction can be found the supplemental materials [40].

The scalar matrix elements  $\langle \bar{q}q \rangle_H \equiv \frac{\langle H | \bar{q}q | H \rangle}{\langle H | H \rangle}$  in the hadron state  $H$  can be obtained from either the direct three point function (3pt) calculation [9, 10, 45–49], or the quark mass dependence of the hadron mass through

the Feynman-Hellman theorem [7, 8, 11–14, 22, 41, 50–62],  $\langle \bar{q}q \rangle_H = \frac{\partial m_H}{\partial m_q}$ . The consistency of the two strategies has been validated for both light and charm quarks in the CLQCD ensembles after performing the continuum extrapolation [28, 29]. Therefore, in this work, we opt for the Feynman-Hellman theorem, which avoids the complications associated with calculating three-point functions. More details can be found in the supplemental materials [40].

Eventually, the total quark mass and trace anomaly

contributions are:

$$\langle H_m \rangle_H = \sum_q \sigma_{qH}, \quad \langle H_a \rangle_H = m_H^{\text{phys}} - \langle H_m \rangle_H, \quad (3)$$

and by subtracting the anomalous quark contributions, the gluon trace anomaly is given by:

$$\langle H_a^g \rangle_H = \langle H_a \rangle_H - \gamma_m \langle H_m \rangle_H. \quad (4)$$

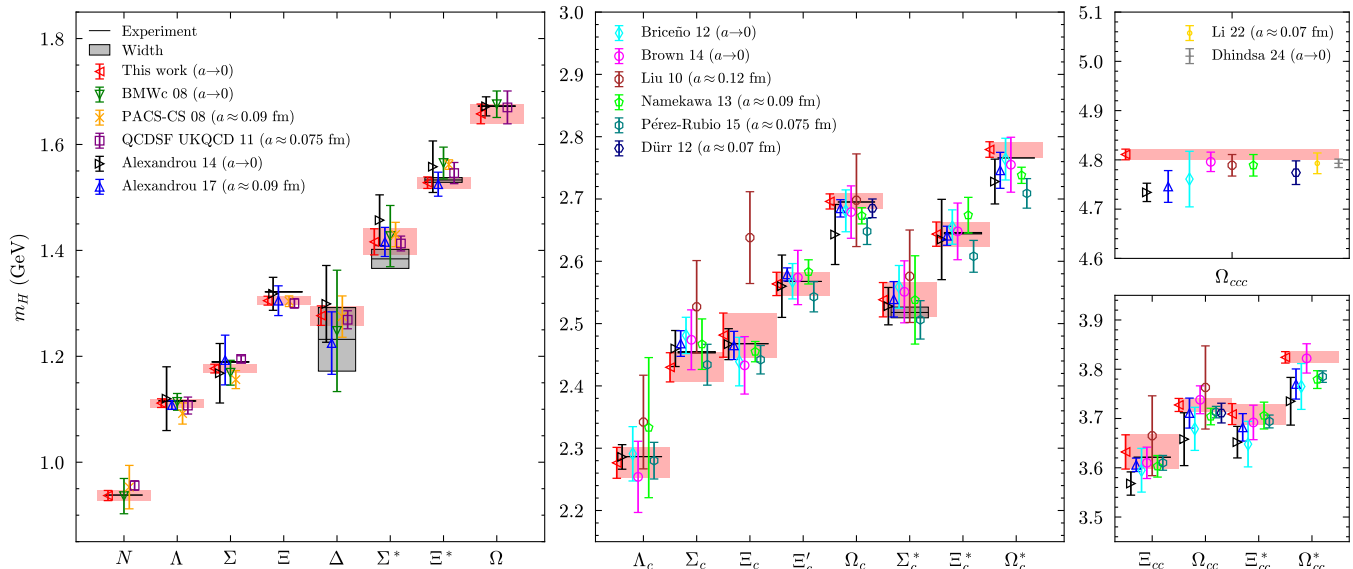


FIG. 3. Comparison of our lattice QCD prediction (red triangles and bands) and those from literature ( BMW 08 [63], PACS-CS 08 [64], QCDSF/UKQCD 11 [65], Alexandrou 14 [13], Alexandrou 17 [66], Briceño 12 [67], Brown 14 [68], Liu 10 [69], Namekawa 13 [70], Perez-Rubio 15 [71], Li 22 [72] and Dhindsa 24 [73])) on the ground-state baryons masses containing 0, 1, 2, and 3 charm quarks, with the experimental values (black band).

*Results:* In Fig. 3, we compare our Lattice QCD predictions for the baryon masses with those in the literature [13, 63–73] and available experimental data. The baryons included in this analysis range from light baryons to heavier charmed and doubly or triply charmed baryons. Our results are represented by the red triangles and bands, while the experimental values are indicated by the black lines. If experimental data is unavailable for certain baryons, the corresponding black bars are omitted. The gray shaded regions represent the experimental decay widths, which are used to account for resonance effects in the measurements. As shown, for the majority of baryons, our predictions are in good agreement with experimental results, particularly for the lower-mass baryons like  $N$ ,  $\Lambda$ , and  $\Sigma$ . For charmed baryons such as  $\Xi_c$  and  $\Omega_c$ , the predictions also align well with experimental data.

Fig. 4 presents the results for the quark  $\sigma$  terms and

the trace anomaly contributions to baryon masses. The upper-left panel shows the light quark  $\sigma$  terms, which represent the direct contributions of light quark masses to the baryon mass. The gray, red, blue, and green triangles indicate baryons with 0, 1, 2, and 3 valence light quarks, respectively. The upper-right and lower-left panels display the  $\sigma$  terms for the strange and charm quarks, respectively, following the same color scheme for quark content. These total strange-quark  $\sigma$  terms are calculated by summing the valence and sea quark contributions, as indicated in Eq. (7). To provide a comprehensive view of the discretization effects across all baryons, additional plots for  $\langle H_m \rangle_H$  are included in the appendix (Fig. 9).

The lower-right panel shows the trace anomaly contribution  $\langle H_a \rangle_H$ , obtained by subtracting the total  $\sigma$  term from the baryon mass according to Eq. (3). This panel also includes the gluon trace anomaly  $\langle H_a^g \rangle_H$  (solid trian-

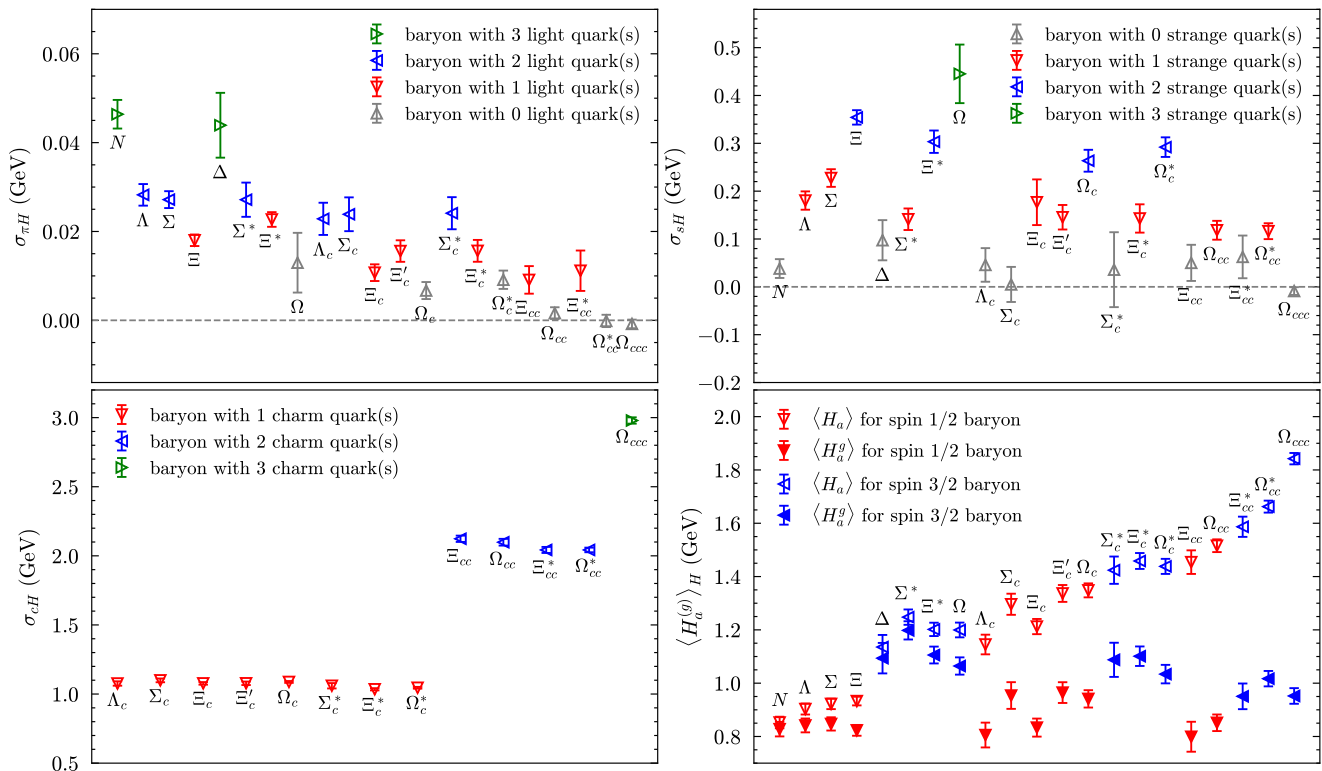


FIG. 4. Results for quark  $\sigma$  terms and trace anomaly contributions to baryon masses. The upper-left, upper-right, and lower-left panels show the  $\sigma$  terms for light, strange, and charm quarks, respectively, with colors indicating the number of valence quarks: gray (0), red (1), blue (2), and green (3). The lower-right panel presents the trace anomaly  $\langle H_a \rangle_H$  and the gluon trace anomaly  $\langle H_a^g \rangle_H$ , with red triangles for spin-1/2 baryons and blue triangles for spin-3/2 baryons.

gles), which is derived by further subtracting the anomalous quark contributions with  $\gamma_m = 0.295$ , as given in Eq. (4). In this panel, red denotes spin-1/2 baryons, and blue denotes spin-3/2 baryons. While the trace anomaly values are similar for light baryons within the spin-1/2 and spin-3/2 groups, the charmed baryons display a clear dependence on the number of charm quarks, with increasing values as the charm content grows. However, after subtracting the anomalous quark mass contributions, the gluon trace anomaly  $\langle H_a^g \rangle$  becomes relatively uniform across spin-1/2 and spin-3/2 baryons, clustering around 1 GeV. Notably, the spin-3/2 baryons show slightly higher gluon trace anomaly contributions compared to their spin-1/2 counterparts.

*Summary:* In this work, we calculated the ground state  $\frac{1}{2}^+$  and  $\frac{3}{2}^+$  baryon masses with the lightest four flavors on 14 ensembles with different lattice spacing, quark masses and volumes. The results were then interpolated to the physical quark masses and extrapolated to the continuum and infinite volume limits. This is the first time that such information has been obtained using ensembles with a uniform setup, effectively controlling all systematic uncertainties except for QED effects.

Using the energy-momentum tensor (EMT) trace sum rule, we provided the first accurate prediction for the trace anomaly contribution of all the baryons studied.

Our findings suggest that the total trace anomaly contribution increases with the number of valence charm quarks. This observation indicates that the quark trace anomaly contribution is significant, especially for heavy quarks. By subtracting this contribution using the quark anomalous dimension  $\gamma_m = 0.295$  at  $\overline{\text{MS}}$  2 GeV with  $N_f = 3$ , we found that the gluon trace anomaly contribution to the baryon states becomes largely insensitive to flavor variations, remaining around 1 GeV with a valence around 10% for different states. Direct calculations of the trace anomaly [23, 24] will be extremely valuable in verifying this prediction without assumption about the quark trace anomaly contribution.

The charm sea quark contribution to the baryon mass is neglected here, not only because our gauge ensemble includes only light and strange quarks, but also due to the heavy quark relation  $m_Q \bar{Q}Q = -\frac{\alpha_s}{12\pi} F^2$  [5, 74], which implies that the heavy sea quark contribution is canceled by the  $N_f$  dependence of the gluon trace anomaly at leading order, leading to the decoupling theorem [75]. In a 2+1-flavor lattice calculation with quenched charm, the charm sigma term in the proton from the disconnected insertion calculation is  $\sim 94(31)$  MeV [47] which gives an estimate of its size. Direct calculations using gauge ensembles with a dynamical charm quark should be beneficial.

After the quark trace anomaly contribution is considered, the sigma terms from the light, strange, and charm quarks are amplified by factors of about 5, 2, and 1.3, respectively, compared to the renormalized quark mass themselves at  $\overline{MS}$  2 GeV. This enhancement suggests that quark-antiquark pairs also contribute significantly to the baryon mass not only from the usual quark loop but also the connected-sea [76] mechanism, with the effects becoming more pronounced as the quark mass decreases.

## ACKNOWLEDGMENT

We thank the CLQCD collaborations for providing us their gauge configurations with dynamical fermions [28], which are generated on HPC Cluster of ITP-CAS, the Southern Nuclear Science Computing Center(SNSC) and the Siyuan-1 cluster supported by the Center for High

Performance Computing at Shanghai Jiao Tong University. We thank Hanyang Xing for providing two-point functions using distillation method for comparison, and Ying Chen, Hengtong Ding, Xu Feng, Chuan Liu, Liming Liu, Zhaofeng Liu, Ji-Hao Wang, Kuan Zhang, and the other CLQCD members for valuable comments and suggestions. The calculations were performed using PyQUDA [77] and Chroma [78] with QUDA [79–81], through HIP programming model [82]. The numerical calculation were carried out on the ORISE Supercomputer, HPC Cluster of ITP-CAS and Advanced Computing East China Sub-center. This work is supported in part by NSFC grants No. 12293060, 12293062, 12435002, 12293065 and 12047503, National Key R&D Program of China No.2024YFE0109800, the Strategic Priority Research Program of Chinese Academy of Sciences, Grant No. XDB34030303 and YSBR-101, and also the science and education integration young faculty project of University of Chinese Academy of Sciences.

- 
- [1] R. L. Workman *et al.* (Particle Data Group), *PTEP* **2022**, 083C01 (2022).
- [2] S. Borsanyi *et al.* (BMW), *Science* **347**, 1452 (2015), [arXiv:1406.4088 \[hep-lat\]](#).
- [3] J. C. Collins, A. Duncan, and S. D. Joglekar, *Phys. Rev. D* **16**, 438 (1977).
- [4] N. K. Nielsen, *Nucl. Phys. B* **120**, 212 (1977).
- [5] M. A. Shifman, A. I. Vainshtein, and V. I. Zakharov, *Phys. Lett.* **B78**, 443 (1978).
- [6] X.-D. Ji, *Phys. Rev. Lett.* **74**, 1071 (1995), [arXiv:hep-ph/9410274](#).
- [7] Y.-B. Yang, J. Liang, Y.-J. Bi, Y. Chen, T. Draper, K.-F. Liu, and Z. Liu, *Phys. Rev. Lett.* **121**, 212001 (2018), [arXiv:1808.08677 \[hep-lat\]](#).
- [8] S. Durr *et al.* (BMW), *Phys. Rev. D* **85**, 014509 (2012), [Erratum: *Phys.Rev.D* 93, 039905 (2016)], [arXiv:1109.4265 \[hep-lat\]](#).
- [9] S. Durr *et al.*, *Phys. Rev. Lett.* **116**, 172001 (2016), [arXiv:1510.08013 \[hep-lat\]](#).
- [10] Y.-B. Yang, A. Alexandru, T. Draper, J. Liang, and K.-F. Liu (xQCD), *Phys. Rev. D* **94**, 054503 (2016), [arXiv:1511.09089 \[hep-lat\]](#).
- [11] G. S. Bali, S. Collins, P. Georg, D. Jenkins, P. Korcyl, A. Schäfer, E. E. Scholz, J. Simeth, W. Söldner, and S. Weishäupl (RQCD), *JHEP* **05**, 035 (2023), [arXiv:2211.03744 \[hep-lat\]](#).
- [12] A. Agadjanov, D. Djukanovic, G. von Hippel, H. B. Meyer, K. Ottnad, and H. Wittig, *Phys. Rev. Lett.* **131**, 261902 (2023), [arXiv:2303.08741 \[hep-lat\]](#).
- [13] C. Alexandrou, V. Drach, K. Jansen, C. Kallionis, and G. Koutsou, *Phys. Rev. D* **90**, 074501 (2014), [arXiv:1406.4310 \[hep-lat\]](#).
- [14] R. Gupta, S. Park, M. Hoferichter, E. Mereghetti, B. Yoon, and T. Bhattacharya, *Phys. Rev. Lett.* **127**, 242002 (2021), [arXiv:2105.12095 \[hep-lat\]](#).
- [15] J. M. Alarcon, J. Martin Camalich, and J. A. Oller, *Phys. Rev. D* **85**, 051503 (2012), [arXiv:1110.3797 \[hep-ph\]](#).
- [16] Y.-H. Chen, D.-L. Yao, and H. Q. Zheng, *Phys. Rev. D* **87**, 054019 (2013), [arXiv:1212.1893 \[hep-ph\]](#).
- [17] M. Hoferichter, J. Ruiz de Elvira, B. Kubis, and U.-G. Meißner, *Phys. Rev. Lett.* **115**, 092301 (2015), [arXiv:1506.04142 \[hep-ph\]](#).
- [18] J. Ruiz de Elvira, M. Hoferichter, B. Kubis, and U.-G. Meißner, *J. Phys. G* **45**, 024001 (2018), [arXiv:1706.01465 \[hep-ph\]](#).
- [19] M. Hoferichter, J. R. de Elvira, B. Kubis, and U.-G. Meißner, *Phys. Lett. B* **843**, 138001 (2023), [arXiv:2305.07045 \[hep-ph\]](#).
- [20] Y. Aoki *et al.* (Flavour Lattice Averaging Group (FLAG)), (2024), [arXiv:2411.04268 \[hep-lat\]](#).
- [21] W. Freeman and D. Toussaint (MILC), *Phys. Rev. D* **88**, 054503 (2013), [arXiv:1204.3866 \[hep-lat\]](#).
- [22] P. Junnarkar and A. Walker-Loud, *Phys. Rev. D* **87**, 114510 (2013), [arXiv:1301.1114 \[hep-lat\]](#).
- [23] F. He, P. Sun, and Y.-B. Yang ( $\chi$ QCD), *Phys. Rev. D* **104**, 074507 (2021), [arXiv:2101.04942 \[hep-lat\]](#).
- [24] B. Wang, F. He, G. Wang, T. Draper, J. Liang, K.-F. Liu, and Y.-B. Yang ( $\chi$ QCD), *Phys. Rev. D* **109**, 094504 (2024), [arXiv:2401.05496 \[hep-lat\]](#).
- [25] K.-F. Liu, *Phys. Lett. B* **849**, 138418 (2024), [arXiv:2302.11600 \[hep-ph\]](#).
- [26] D. C. Hackett, D. A. Pefkou, and P. E. Shanahan, *Phys. Rev. Lett.* **132**, 251904 (2024), [arXiv:2310.08484 \[hep-lat\]](#).
- [27] D. C. Hackett, P. R. Oare, D. A. Pefkou, and P. E. Shanahan, *Phys. Rev. D* **108**, 114504 (2023), [arXiv:2307.11707 \[hep-lat\]](#).
- [28] Z.-C. Hu *et al.* (CLQCD), *Phys. Rev. D* **109**, 054507 (2024), [arXiv:2310.00814 \[hep-lat\]](#).
- [29] H.-Y. Du *et al.* (CLQCD), (2024), [arXiv:2408.03548 \[hep-lat\]](#).
- [30] Y. Aoki *et al.* (Flavour Lattice Averaging Group (FLAG)), *Eur. Phys. J. C* **82**, 869 (2022), [arXiv:2111.09849 \[hep-lat\]](#).
- [31] H. Xing, J. Liang, L. Liu, P. Sun, and Y.-B. Yang, (2022), [arXiv:2210.08555 \[hep-lat\]](#).

- [32] H. Liu, J. He, L. Liu, P. Sun, W. Wang, Y.-B. Yang, and Q.-A. Zhang, *Sci. China Phys. Mech. Astron.* **67**, 211011 (2024), [arXiv:2207.00183 \[hep-lat\]](#).
- [33] H. Liu, L. Liu, P. Sun, W. Sun, J.-X. Tan, W. Wang, Y.-B. Yang, and Q.-A. Zhang, *Phys. Lett. B* **841**, 137941 (2023), [arXiv:2303.17865 \[hep-lat\]](#).
- [34] H. Liu, W. Wang, and Q.-A. Zhang, *Phys. Rev. D* **109**, 036037 (2024), [arXiv:2309.05432 \[hep-ph\]](#).
- [35] H. Yan, C. Liu, L. Liu, Y. Meng, and H. Xing, (2024), [arXiv:2404.13479 \[hep-lat\]](#).
- [36] Q.-A. Zhang *et al.*, *Chin. Phys. C* **46**, 011002 (2022), [arXiv:2103.07064 \[hep-lat\]](#).
- [37] X.-Y. Han, J. Hua, X. Ji, C.-D. Lü, W. Wang, J. Xu, Q.-A. Zhang, and S. Zhao, (2024), [arXiv:2403.17492 \[hep-ph\]](#).
- [38] Y. Meng, J.-L. Dang, C. Liu, Z. Liu, T. Shen, H. Yan, and K.-L. Zhang, *Phys. Rev. D* **109**, 074511 (2024), [arXiv:2401.13475 \[hep-lat\]](#).
- [39] Y. Meng, J.-L. Dang, C. Liu, X.-Y. Tuo, H. Yan, Y.-B. Yang, and K.-L. Zhang, *Phys. Rev. D* **110**, 074510 (2024), [arXiv:2407.13568 \[hep-lat\]](#).
- [40] Supplemental materials.
- [41] S. Borsanyi, Z. Fodor, C. Hoelbling, L. Lellouch, K. K. Szabo, C. Torrero, and L. Varnhorst, (2020), [arXiv:2007.03319 \[hep-lat\]](#).
- [42] B. C. Tiburzi, *Phys. Rev. D* **72**, 094501 (2005), [Erratum: *Phys.Rev.D* 79, 039904 (2009)], [arXiv:hep-lat/0508019](#).
- [43] S. Borsanyi *et al.*, *Nature* **593**, 51 (2021), [arXiv:2002.12347 \[hep-lat\]](#).
- [44] M. Di Carlo, D. Giusti, V. Lubicz, G. Martinelli, C. T. Sachrajda, F. Sanfilippo, S. Simula, and N. Tantalo, *Phys. Rev. D* **100**, 034514 (2019), [arXiv:1904.08731 \[hep-lat\]](#).
- [45] C. Alexandrou, S. Bacchio, M. Constantinou, J. Finkenrath, K. Hadjiyiannakou, K. Jansen, G. Koutsou, and A. Vaquero Aviles-Casco, *Phys. Rev. D* **102**, 054517 (2020), [arXiv:1909.00485 \[hep-lat\]](#).
- [46] G. S. Bali, S. Collins, D. Richtmann, A. Schäfer, W. Söldner, and A. Sternbeck (RQCD), *Phys. Rev. D* **93**, 094504 (2016), [arXiv:1603.00827 \[hep-lat\]](#).
- [47] M. Gong *et al.* (XQCD), *Phys. Rev. D* **88**, 014503 (2013), [arXiv:1304.1194 \[hep-ph\]](#).
- [48] A. Abdel-Rehim, C. Alexandrou, M. Constantinou, K. Hadjiyiannakou, K. Jansen, C. Kallidonis, G. Koutsou, and A. Vaquero Aviles-Casco (ETM), *Phys. Rev. Lett.* **116**, 252001 (2016), [arXiv:1601.01624 \[hep-lat\]](#).
- [49] G. S. Bali *et al.* (QCDSF), *Phys. Rev. D* **85**, 054502 (2012), [arXiv:1111.1600 \[hep-lat\]](#).
- [50] P. M. Copeland, C.-R. Ji, and W. Melnitchouk, *Phys. Rev. D* **107**, 094041 (2023), [arXiv:2112.03198 \[nucl-th\]](#).
- [51] M. Frink and U.-G. Meissner, *JHEP* **07**, 028 (2004), [arXiv:hep-lat/0404018](#).
- [52] J. Martin Camalich, L. S. Geng, and M. J. Vicente Vacas, *Phys. Rev. D* **82**, 074504 (2010), [arXiv:1003.1929 \[hep-lat\]](#).
- [53] K. I. Ishikawa *et al.* (PACS-CS), *Phys. Rev. D* **80**, 054502 (2009), [arXiv:0905.0962 \[hep-lat\]](#).
- [54] X.-L. Ren, L.-S. Geng, and J. Meng, *Phys. Rev. D* **91**, 051502 (2015), [arXiv:1404.4799 \[hep-ph\]](#).
- [55] X. L. Ren, L. S. Geng, J. Martin Camalich, J. Meng, and H. Toki, *JHEP* **12**, 073 (2012), [arXiv:1209.3641 \[nucl-th\]](#).
- [56] A. Semke and M. F. M. Lutz, *Phys. Lett. B* **717**, 242 (2012), [arXiv:1202.3556 \[hep-ph\]](#).
- [57] R. D. Young and A. W. Thomas, *Nucl. Phys. A* **844**, 266C (2010), [arXiv:0911.1757 \[hep-lat\]](#).
- [58] L. Alvarez-Ruso, T. Ledwig, J. Martin Camalich, and M. J. Vicente-Vacas, *Phys. Rev. D* **88**, 054507 (2013), [arXiv:1304.0483 \[hep-ph\]](#).
- [59] R. Horsley, Y. Nakamura, H. Perlt, D. Pleiter, P. E. L. Rakow, G. Schierholz, A. Schiller, H. Stuben, F. Winter, and J. M. Zanotti (QCDSF-UKQCD), *Phys. Rev. D* **85**, 034506 (2012), [arXiv:1110.4971 \[hep-lat\]](#).
- [60] C. S. An and B. Saghai, *Phys. Rev. D* **92**, 014002 (2015), [arXiv:1404.2389 \[hep-ph\]](#).
- [61] K. Takeda, S. Aoki, S. Hashimoto, T. Kaneko, J. Noaki, and T. Onogi (JLQCD), *Phys. Rev. D* **83**, 114506 (2011), [arXiv:1011.1964 \[hep-lat\]](#).
- [62] D. Toussaint and W. Freeman (MILC), *Phys. Rev. Lett.* **103**, 122002 (2009), [arXiv:0905.2432 \[hep-lat\]](#).
- [63] S. Durr *et al.* (BMW), *Science* **322**, 1224 (2008), [arXiv:0906.3599 \[hep-lat\]](#).
- [64] S. Aoki *et al.* (PACS-CS), *Phys. Rev. D* **79**, 034503 (2009), [arXiv:0807.1661 \[hep-lat\]](#).
- [65] W. Bietenholz *et al.*, *Phys. Rev. D* **84**, 054509 (2011), [arXiv:1102.5300 \[hep-lat\]](#).
- [66] C. Alexandrou and C. Kallidonis, *Phys. Rev. D* **96**, 034511 (2017), [arXiv:1704.02647 \[hep-lat\]](#).
- [67] R. A. Briceno, H.-W. Lin, and D. R. Bolton, *Phys. Rev. D* **86**, 094504 (2012), [arXiv:1207.3536 \[hep-lat\]](#).
- [68] Z. S. Brown, W. Detmold, S. Meinel, and K. Orginos, *Phys. Rev. D* **90**, 094507 (2014), [arXiv:1409.0497 \[hep-lat\]](#).
- [69] L. Liu, H.-W. Lin, K. Orginos, and A. Walker-Loud, *Phys. Rev. D* **81**, 094505 (2010), [arXiv:0909.3294 \[hep-lat\]](#).
- [70] Y. Namekawa *et al.* (PACS-CS), *Phys. Rev. D* **87**, 094512 (2013), [arXiv:1301.4743 \[hep-lat\]](#).
- [71] P. Pérez-Rubio, S. Collins, and G. S. Bali, *Phys. Rev. D* **92**, 034504 (2015), [arXiv:1503.08440 \[hep-lat\]](#).
- [72] J.-B. Li, L.-C. Gui, W. Sun, J. Liang, and W. Qin, (2022), [arXiv:2211.04713 \[hep-lat\]](#).
- [73] N. S. Dhindsa, D. Chakraborty, A. Radhakrishnan, N. Mathur, and M. Padmanath, (2024), [arXiv:2411.12729 \[hep-lat\]](#).
- [74] R. Tarrach, *Nucl. Phys.* **B196**, 45 (1982).
- [75] T. Appelquist and J. Carazzone, *Phys. Rev. D* **11**, 2856 (1975).
- [76] K.-F. Liu, W.-C. Chang, H.-Y. Cheng, and J.-C. Peng, *Phys. Rev. Lett.* **109**, 252002 (2012), [arXiv:1206.4339 \[hep-ph\]](#).
- [77] X. Jiang, C. Shi, Y. Chen, M. Gong, and Y.-B. Yang, (2024), [arXiv:2411.08461 \[hep-lat\]](#).
- [78] R. G. Edwards and B. Joo (SciDAC, LHPC, UKQCD), *Lattice field theory. Proceedings, 22nd International Symposium, Lattice 2004, Batavia, USA, June 21-26, 2004*, *Nucl. Phys. Proc. Suppl.* **140**, 832 (2005), [832(2004)], [arXiv:hep-lat/0409003 \[hep-lat\]](#).
- [79] M. A. Clark, R. Babich, K. Barros, R. C. Brower, and C. Rebbi, *Comput. Phys. Commun.* **181**, 1517 (2010), [arXiv:0911.3191 \[hep-lat\]](#).
- [80] R. Babich, M. A. Clark, B. Joo, G. Shi, R. C. Brower, and S. Gottlieb, in *SC11 International Conference for High Performance Computing, Networking, Storage and Analysis Seattle, Washington, November 12-18, 2011* (2011) [arXiv:1109.2935 \[hep-lat\]](#).
- [81] M. A. Clark, B. Jo, A. Strelchenko, M. Cheng, A. Gambhir, and R. Brower, (2016), [arXiv:1612.07873 \[hep-lat\]](#).

- [82] Y.-J. Bi, Y. Xiao, M. Gong, W.-Y. Guo, P. Sun, S. Xu, and Y.-B. Yang, *Proceedings, 37th International Symposium on Lattice Field Theory (Lattice 2019): Wuhan, China, June 16-22 2019*, PoS **LATTICE2019**, 286 (2020), [arXiv:2001.05706 \[hep-lat\]](#).
- [83] T. Ishikawa *et al.* (JLQCD), *Phys. Rev. D* **78**, 011502 (2008), [arXiv:0704.1937 \[hep-lat\]](#).



Baryon Quark Content		Interpolating Field	$I$	$I_z$	$J$
$p$	$uud$	$\epsilon_{abc}P^+(d_a^T C \gamma^5 u_b)u_c$	$\frac{1}{2}$	$+\frac{1}{2}$	
$\Lambda$	$uds$	$\epsilon_{abc}P^+[2(u_a^T C \gamma^5 d_b)s_c + (u_a^T C \gamma^5 s_b)d_c - (d_a^T C \gamma^5 s_b)u_c]$	0	0	
$\Sigma^+$	$uus$	$\epsilon_{abc}P^+(s_a^T C \gamma^5 u_b)u_c$	1	+1	
$\Xi^0$	$uss$	$\epsilon_{abc}P^+(u_a^T C \gamma^5 s_b)s_c$	$\frac{1}{2}$	$+\frac{1}{2}$	
$\Lambda_c$	$udc$	$\epsilon_{abc}P^+[2(u_a^T C \gamma^5 d_b)c_c + (u_a^T C \gamma^5 c_b)d_c - (d_a^T C \gamma^5 c_b)u_c]$	0	0	
$\Sigma_c^{++}$	$uuc$	$\epsilon_{abc}P^+(c_a^T C \gamma^5 u_b)u_c$	1	+1	$\frac{1}{2}$
$\Xi_c^+$	$usc$	$\epsilon_{abc}P^+[2(u_a^T C \gamma^5 s_b)c_c + (u_a^T C \gamma^5 c_b)s_c - (s_a^T C \gamma^5 c_b)u_c]$	$\frac{1}{2}$	$+\frac{1}{2}$	
$\Xi_c'^+$	$usc$	$\epsilon_{abc}P^+[(u_a^T C \gamma^5 c_b)s_c + (s_a^T C \gamma^5 c_b)u_c]$	$\frac{1}{2}$	$+\frac{1}{2}$	
$\Omega_c^0$	$ssc$	$\epsilon_{abc}P^+(c_a^T C \gamma^5 s_b)s_c$	0	0	
$\Xi_{cc}^{++}$	$ucc$	$\epsilon_{abc}P^+(u_a^T C \gamma^5 c_b)c_c$	$\frac{1}{2}$	$+\frac{1}{2}$	
$\Omega_{cc}^+$	$scc$	$\epsilon_{abc}P^+(s_a^T C \gamma^5 c_b)c_c$	0	0	
$\Delta^{++}$	$uuu$	$\epsilon_{abc}P^+(u_a^T C \gamma^\mu u_b)u_c$	$\frac{3}{2}$	$+\frac{3}{2}$	
$\Sigma^{*+}$	$uus$	$\epsilon_{abc}P^+[(u_a^T C \gamma^\mu u_b)s_c + 2(s_a^T C \gamma^\mu u_b)u_c]$	1	+1	
$\Xi^{*0}$	$uss$	$\epsilon_{abc}P^+[2(s_a^T C \gamma^\mu u_b)s_c + (s_a^T C \gamma^\mu s_b)u_c]$	$\frac{1}{2}$	$+\frac{1}{2}$	
$\Omega^-$	$sss$	$\epsilon_{abc}P^+(s_a^T C \gamma^\mu s_b)s_c$	0	0	
$\Xi_c^{*+}$	$usc$	$\epsilon_{abc}P^+[(u_a^T C \gamma^\mu s_b)c_c + (s_a^T C \gamma^\mu c_b)u_c + (c_a^T C \gamma^\mu u_b)s_c]$	$\frac{1}{2}$	$+\frac{1}{2}$	$\frac{3}{2}$
$\Omega_c^{*0}$	$ssc$	$\epsilon_{abc}P^+[2(s_a^T C \gamma^\mu c_b)s_c + (s_a^T C \gamma^\mu s_b)c_c]$	0	0	
$\Sigma_c^{*++}$	$uuc$	$\epsilon_{abc}P^+[(u_a^T C \gamma^\mu u_b)c_c + 2(c_a^T C \gamma^\mu u_b)u_c]$	1	+1	
$\Xi_{cc}^{*++}$	$ucc$	$\epsilon_{abc}P^+[2(c_a^T C \gamma^\mu u_b)c_c + (c_a^T C \gamma^\mu c_b)u_c]$	$\frac{1}{2}$	$+\frac{1}{2}$	
$\Omega_{cc}^{*+}$	$scc$	$\epsilon_{abc}P^+[2(c_a^T C \gamma^\mu s_b)c_c + (c_a^T C \gamma^\mu c_b)s_c]$	0	0	
$\Omega_{ccc}^{++}$	$ccc$	$\epsilon_{abc}P^+(c_a^T C \gamma^\mu c_b)c_c$	0	0	

TABLE II. Interpolating fields for baryons.

## SUPPLEMENTAL MATERIALS

### 1. Interpolation fields and two point functions

The interpolation fields for the baryons we investigated in this work are summarized in Table II. Taking the nucleon as example, the the wall-to-point two-point functions we used in the this study is constructed below, explicitly recovering the coordinate and Dirac indices,

$$\begin{aligned}
C_{2,N}^{wp}(y^0, x^0) &= \sum_{\vec{x}, \vec{y}} \langle \chi_N^\alpha(y) \bar{\chi}_N^\alpha(x) \rangle = \sum_{\vec{y}} \epsilon_{abc} \epsilon_{a'b'c'} \left\langle (C\gamma_5)^{\alpha'\beta'} (C\gamma_5)^{\alpha\beta} (P^\pm)^{\gamma\gamma'} S_a^C(y, x^0)_{\alpha'a} \right. \\
&\quad \left. \times \left[ S_u^C(y, x^0)_{\beta'\beta} S_u^C(y, x^0)_{\gamma'\gamma} - S_u^C(y, x^0)_{\beta'\gamma} S_u^C(y, x^0)_{\gamma'\beta} \right] \right\rangle \quad (5)
\end{aligned}$$

where the Coulomb gauge-fixed wall propagator is defined by  $S_f^C(y, x^0) \equiv \sum_{\vec{x}} S(y, x; U_C; \tilde{m}_f^b)$  as used in Ref. [28], and  $S(y, x; U_C) = \psi(y; U_C) \bar{\psi}(x; U_C)$  is the standard quark propagator computed with the gauge configuration  $U$ . The Coulomb gauge-fixed configuration  $U_C$  satisfies the discretized gauge-fixing condition  $\text{Im} \left[ \sum_{i=1}^3 (U_C(x) - U_C(x - a\hat{n}_i)) \right] = 0$ .

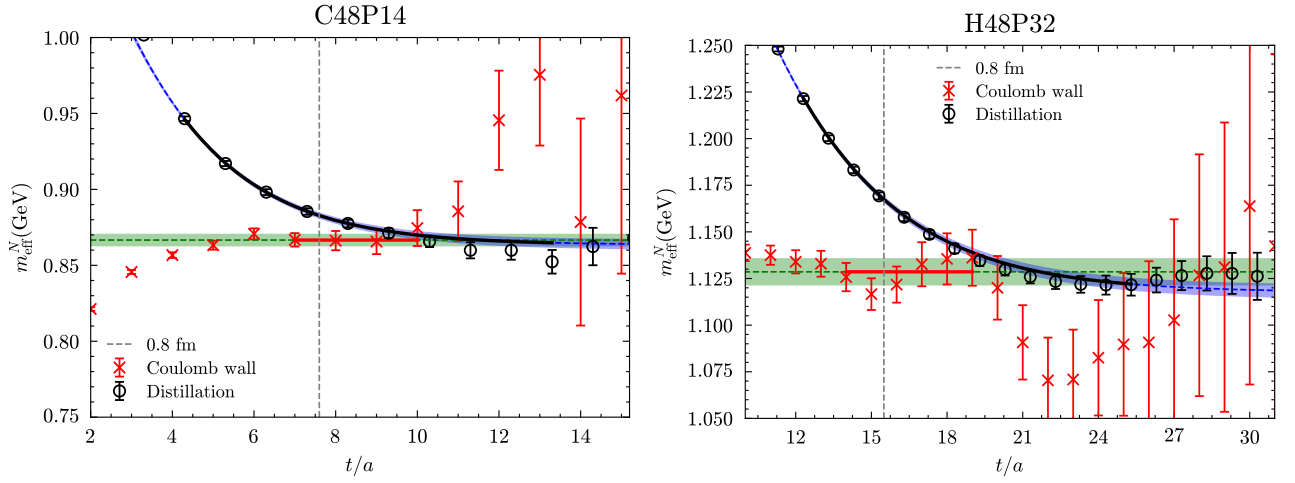


FIG. 5. The effective mass obtained from the two-point correlation functions (2pt) of the nucleon in two representative ensembles: the physical point ensemble C48P14 (left panel) and the ensemble with the finest lattice spacing, H48P32 (right panel). The effective mass derived from the 2pt correlation functions (using a Coulomb wall source and point sink, indicated by red crosses) is compared with the results obtained using the distillation method (shown as black circles). Both methods exhibit good agreement in the plateau region, despite different initial trends with respect to  $t/a$ . The green bands represent the ground state mass that we extracted.

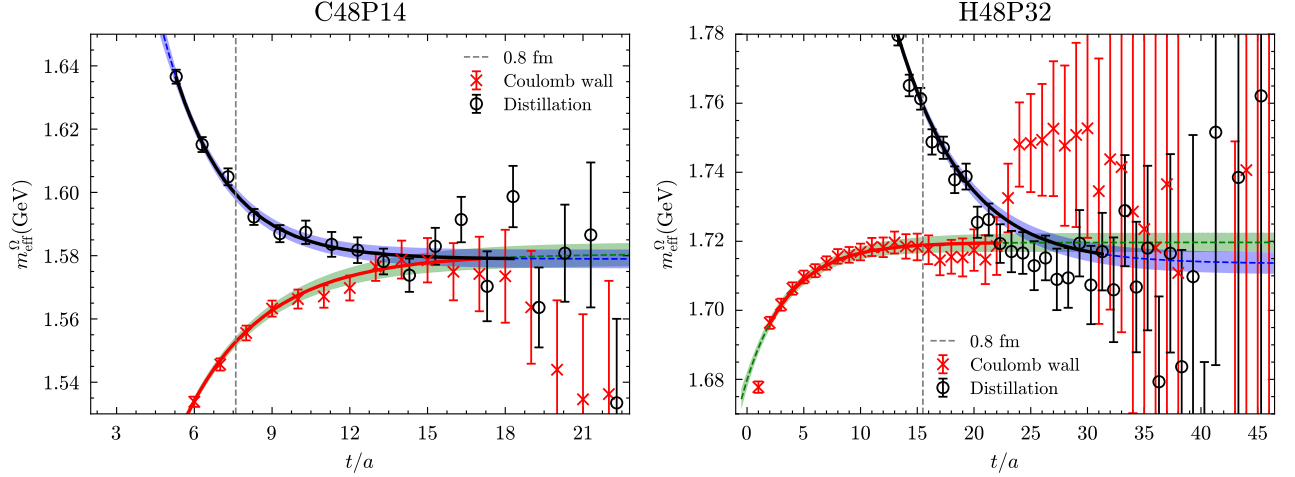


FIG. 6. Similar figures for the  $\Omega$  baryon.

## 2. Ground state baryon mass extraction

In Fig. 5-7, we present the effective logarithmic mass obtained from two-point correlators for three baryons—the nucleon,  $\Omega$ , and  $\Omega_c$ —on two representative ensembles: the physical point ensemble C48P14 and the finest lattice spacing ensemble H48P32. The results are shown using the Coulomb wall source (red crosses) and, where available, the distillation method (black circles) from CLQCD collaborators.

For both the nucleon and  $\Omega$  baryons, we observe that the effective masses from the Coulomb wall source and distillation method are in good agreement once the plateau is reached, even though the initial trends with respect to  $t/a$  differ; specifically, the Coulomb wall source tends to increase with  $t$ , while the distillation results exhibit a decrease before stabilizing. This consistency at the plateau confirms the reliability of both approaches. Notably, no comparative distillation data is available for the  $\Omega_c$  baryon. The green bands in each plot indicate the fit uncertainties for the extracted mass values, showing robust consistency across methods and ensembles.

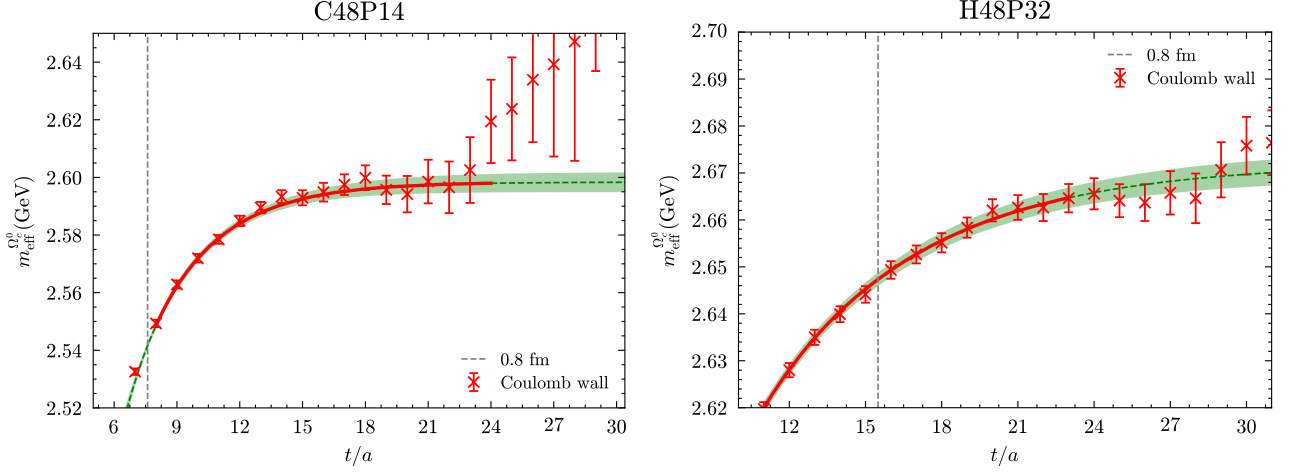


FIG. 7. Similar figures for the  $\Omega_c$  baryon, while the distillation case is not available.

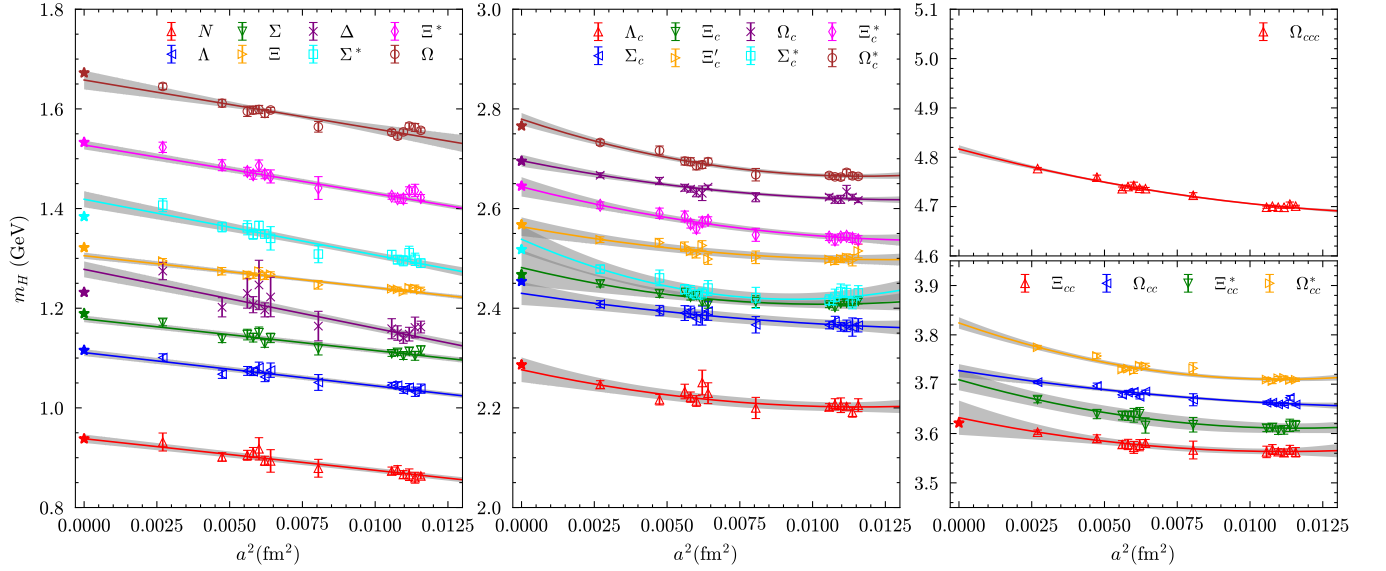


FIG. 8. Fitting results for the masses of all baryons, showing their dependence on lattice spacing  $a^2$ . For light baryons, an  $a^2$  extrapolation is applied, while for charmed baryons, an  $a^4$  extrapolation is used where necessary. The gray bands represent fit uncertainties, and colored stars indicate experimental values when available. All data points have been corrected for non-physical effects using the global fit, demonstrating consistent treatment of discretization effects across the baryon spectrum.

In Fig. 8, we show the fitting results for the masses of all baryons, with each plot illustrating the dependence on lattice spacing  $a^2$ . For light baryons, we apply an  $a^2$  extrapolation, while for charmed baryons, an  $a^4$  extrapolation is used to capture higher-order discretization effects. Each data point has been adjusted for other non-physical effects (nonphysical quark masses and finite volume correction) using the global fit. The gray bands represent the uncertainties from the fits, providing a visual indication of the extrapolation reliability. Colored stars indicate experimental values when available, serving as a benchmark for our Lattice QCD predictions.

### 3. $\sigma_{qH}$ extraction

Thus the light quark contribution, namely the  $\sigma_{\pi H}$ , are obtained using the leading order  $\chi$ PT relation  $m_\pi^2 \propto m_l$ ,

$$\sigma_{\pi H} = m_l \frac{\partial m_H}{\partial m_l} = \frac{m_\pi}{2} \frac{\partial m_H}{\partial m_\pi} \Big|_{m_\pi^{\text{val/pc}} = m_\pi^{\text{phys}}}, \quad (6)$$

where  $m_H(m_\pi^{\text{val}}, m_\pi^{\text{sea}}, m_{\eta_s}^{\text{sea}})$  is parameterized using Eq. (2). The next leading order correction of  $\chi$ PT is around 2% within the range of pion masses we considered [28] and then can be safely ignored in light of the statistical uncertainty of  $\sigma_{\pi H}$ .

The contribution of the strange quark is divided into two components,

$$\sigma_{sH} = \frac{m_{\eta_s}}{2} \frac{\partial m_H}{\partial m_{\eta_s}^{\text{sea}}} + \sigma_{sH}^{\text{val}}, \quad (7)$$

where the first term represents the strange sea contribution, based on the consistency of  $m_{\eta_s}^2/m_s$  with a constant value of 4.9(1) around the physical strange quark mass [28]. Meanwhile, the valence strange quark contribution  $\sigma_{sH}^{\text{val}}$  is extracted using a different strategy that provides better control over kinds of systematic uncertainties. First, we obtain the multiplicatively renormalizable strange quark mass  $m_s^{\text{PC}}$  through the partially conserved axial current (PCAC) relation [83] for each of the three valence strange quark masses. We then interpolate  $\sigma_{sH}^{\text{val}} = m_s^{\text{val,PC}} \frac{\partial m_H}{\partial m_s^{\text{val,PC}}}$  to the valence strange quark mass  $m_s^{\text{val,PC}}$  corresponds to the ‘‘physical’’  $\eta_s$  mass. Next, we perform a joint fit,

$$\begin{aligned} \sigma_{sH}^{\text{val}}(m_\pi, m_{\eta_s}, a, 1/L) &= \sigma_{sH}^{\text{val}}(m_\pi^{\text{phys}}, m_{\eta_s}^{\text{phys}}, 0, 0) \\ &+ d_1(m_\pi^2 - (m_\pi^{\text{phys}})^2) + d_2(m_{\eta_s, \text{sea}}^2 - (m_{\eta_s}^{\text{phys}})^2) \\ &+ d_3 a^2 + d_5 e^{-m_\pi L}, \end{aligned} \quad (8)$$

to eliminate contamination from nonphysical light and strange sea quark masses, as well as finite volume effects. For the  $\sigma_{sH}^{\text{val}}$  in the charmed baryon, the valence charm quark mass is also interpolated to that correspond to the pure QCD  $D_s$  mass, and additional  $a^4$  term is added to control the discretization error properly. The contribution from the valence charm quark can be obtained in a similar manner, and the sea charm quark contribution is neglected since it is canceled by the flavor dependence of the gluon trace anomaly at the leading order [5, 74].

In Fig. 9, we present the plots of  $\langle H_m \rangle_H$  for all baryons, similar to Fig. 8. As indicated in the figure, the discretization effects on  $\langle H_m \rangle_H$  are generally smaller than those on the total baryon mass, highlighting the stability of  $\langle H_m \rangle_H$  under different lattice spacings.

In table III, we summarized the final numerical results of the baryon masses, sigma terms and also trace anomaly contributions.

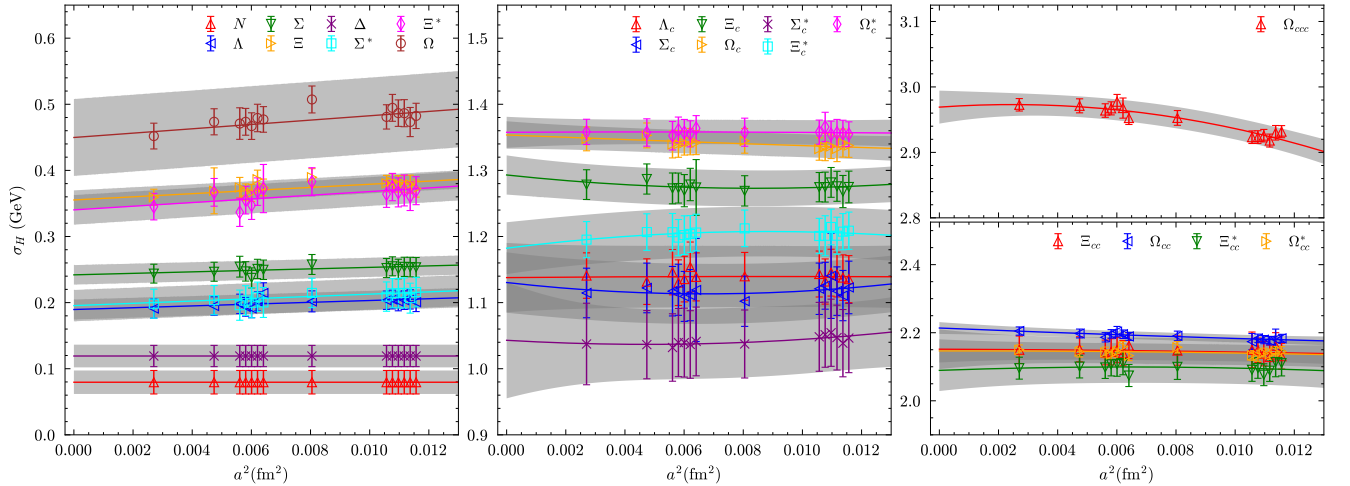


FIG. 9. Similar to Fig. 8 but for  $\langle H_m \rangle_H$ . The plots indicate that the discretization effects on  $\langle H_m \rangle_H$  are generally smaller than those observed for the baryon masses, though the associated uncertainties are comparatively larger.

Baryon	Quarks	$J^P$	$m_H$	$\sigma_{\pi H}$	$\sigma_{sH}$	$\sigma_{cH}^{\text{val}}$	$\langle H_a \rangle_H$	$\langle H_a^g \rangle_H$
$N$	$uud$	$\frac{1}{2}^+$	0.9371(87)	0.0464(32)	0.038(20)	0	0.85(17)	0.828(27)
$\Lambda$	$uds$	$\frac{1}{2}^+$	1.1116(72)	0.0282(24)	0.180(19)	0	0.90(42)	0.841(26)
$\Sigma$	$uus$	$\frac{1}{2}^+$	1.1769(66)	0.0272(19)	0.227(18)	0	0.92(51)	0.847(25)
$\Xi$	$uss$	$\frac{1}{2}^+$	1.3051(65)	0.0180(13)	0.354(15)	0	0.93(75)	0.823(20)
$\Delta$	$uuu$	$\frac{3}{2}^+$	1.277(16)	0.0439(73)	0.097(42)	0	1.14(29)	1.094(56)
$\Sigma^*$	$uus$	$\frac{3}{2}^+$	1.416(18)	0.0272(39)	0.141(23)	0	1.25(35)	1.198(31)
$\Xi^*$	$uss$	$\frac{3}{2}^+$	1.5279(88)	0.0227(17)	0.303(23)	0	1.20(65)	1.106(32)
$\Omega$	$sss$	$\frac{3}{2}^+$	1.658(19)	0.0130(67)	0.445(61)	0	1.20(96)	1.064(71)
$\Lambda_c$	$udc$	$\frac{1}{2}^+$	2.277(25)	0.0228(36)	0.046(35)	1.076(16)	1.145(37)	0.805(47)
$\Sigma_c$	$uuc$	$\frac{1}{2}^+$	2.430(23)	0.0239(38)	0.005(37)	1.099(14)	1.296(41)	0.954(51)
$\Xi_c$	$usc$	$\frac{1}{2}^+$	2.482(27)	0.0107(19)	0.177(48)	1.0771(93)	1.212(29)	0.833(38)
$\Xi'_c$	$usc$	$\frac{1}{2}^+$	2.564(17)	0.0156(24)	0.145(26)	1.078(13)	1.337(32)	0.965(39)
$\Omega_c$	$ssc$	$\frac{1}{2}^+$	2.696(12)	0.0067(19)	0.264(23)	1.0875(67)	1.348(27)	0.941(34)
$\Sigma_c^*$	$uuc$	$\frac{3}{2}^+$	2.538(28)	0.0241(36)	0.036(78)	1.060(19)	1.424(67)	1.088(91)
$\Xi_c^*$	$usc$	$\frac{3}{2}^+$	2.644(19)	0.0156(25)	0.143(30)	1.0344(80)	1.458(30)	1.101(37)
$\Omega_c^*$	$ssc$	$\frac{3}{2}^+$	2.779(12)	0.0091(21)	0.292(20)	1.0454(63)	1.438(28)	1.034(35)
$\Xi_{cc}$	$ucc$	$\frac{1}{2}^+$	3.632(35)	0.0091(31)	0.050(38)	2.123(23)	1.454(45)	0.799(58)
$\Omega_{cc}$	$scc$	$\frac{1}{2}^+$	3.7275(94)	0.0016(13)	0.118(20)	2.098(24)	1.516(24)	0.851(31)
$\Xi_{cc}^*$	$ucc$	$\frac{3}{2}^+$	3.709(21)	0.0112(45)	0.063(45)	2.043(22)	1.587(44)	0.951(57)
$\Omega_{cc}^*$	$scc$	$\frac{3}{2}^+$	3.8241(99)	-0.0001(14)	0.116(17)	2.043(17)	1.662(24)	1.017(31)
$\Omega_{ccc}$	$ccc$	$\frac{3}{2}^+$	4.8110(97)	-0.00081(97)	-0.0088(81)	2.979(23)	1.842(22)	0.952(30)

TABLE III. Numerical results of the baryon masses and contributions from the quark mass and trace anomaly.